

High-Dimensional Bayesian Optimization with Manifold Gaussian Processes

Riccardo Moriconi ^{*1} K. S. Sesh Kumar ^{*1} Marc P. Deisenroth ^{*1}

Abstract

Bayesian optimization (BO) is a powerful approach for seeking the global optimum of expensive black-box functions and has proven successful for fine tuning hyper-parameters of machine learning models. The Bayesian optimization routine involves learning a response surface and maximizing a score to select the most valuable inputs to be queried at the next iteration. These key steps are subject to the curse of dimensionality so that Bayesian optimization does not scale beyond 10–20 parameters. In this work, we address this issue and propose a high-dimensional BO method that learns a nonlinear low-dimensional manifold of the input space. We achieve this with a multi-layer neural network embedded in the covariance function of a Gaussian process. This approach applies unsupervised dimensionality reduction as a byproduct of a supervised regression solution. This also allows exploiting data efficiency of Gaussian process models in a Bayesian framework. We also introduce a nonlinear mapping from the manifold to the high-dimensional space based on multi-output Gaussian processes and jointly train it end-to-end via marginal likelihood maximization. We show this intrinsically low-dimensional optimization outperforms recent baselines in high-dimensional BO literature on a set of benchmark functions in 60 dimensions.

1. Introduction

Using machine learning (ML) algorithms requires a wise selection of tunable hyper-parameters and model design choices that is usually left to computer scientists and statisticians. With the increase of use of the ML algorithms among non experts in the field there is a rising need for automatizing this tedious sequential design process. The evaluation of per-

formance of these parameters may involve costly and time-consuming training procedures. Moreover, the relationship between the model parameters and performance measurements may lack analytic expressions and is therefore considered as a black box. In this context, Bayesian optimization has emerged as model-based strategy for sample-efficient global optimization of expensive black box functions (Jones et al., 1998; Kushner, 1964; Močkus, 1975). The key components are (i) a probabilistic surrogate model (response surface) that predicts values of the black-box objective function with uncertainty and (ii) a score/acquisition function that defines an exploration strategy based on the model’s predictive distribution. The surrogate model is used as a proxy for the expensive black-box evaluation procedure. The acquisition function, instead, defines a utility to be maximized in order to identify where to evaluate next the expensive objective function. Bayesian optimization has successfully been applied in automated tuning of machine learning algorithms (Snoek et al., 2012), movie recommendation systems (Sui et al., 2015) and software configuration (Hutter et al., 2011). Despite many successes this model-based approach suffers from the curse of dimensionality both for learning the surrogate model and for optimizing the acquisition function.

Learning a high-dimensional response surface is notoriously hard (Garnett et al., 2013; Rana et al., 2017). Distances between inputs easily become large and function values at highly distant points easily become uncorrelated. As a result, the optimization landscape is characterized by flat regions where the optimization of the resulting acquisition function with gradient-based methods (Lu et al., 1994; Zhu et al., 1997) is hard. Moreover, the highly non-convex optimization surface identified by the acquisition function requires an exponential number of evaluations in the number of dimensions representing the key bottleneck for Bayesian optimization in high dimensions.

A common assumption in the high-dimensional Bayesian optimization literature is that the objective function varies on a linear subspace of dimensionality $d \ll D$, where D is the dimensionality of the original input space. Chen et al. (2012) select axis-aligned *active* dimensions, that is coordinates that are actually relevant for optimization. A budget of samples is allocated to discriminate these active dimensions based on a hypothesis testing approach.

^{*}Equal contribution ¹Department of Computing, Imperial College London, London, United Kingdom. Correspondence to: Riccardo Moriconi <r.moriconi16@imperial.ac.uk>, Sesh Kumar <s.karri@imperial.ac.uk>, Marc P. Deisenroth <m.deisenroth@imperial.ac.uk>.

Djolonga et al. (2013) learn a linear mapping using low-rank recovery algorithms allocating a set of inputs to subspace learning. Wang et al. (2013) propose *random embedding* BO (REMBO) which restrict the search to a random linear subspace while deriving bounds in embedded space that are proven to contain the optimum with high probability. In this work, the linear mapping for dimensionality reduction is represented by a random matrix with Gaussian samples as entries. However, implementation-wise, it requires further cleverness to account for non-injectivity of the mapping from the embedding to the original domain. In our work based on manifold learning, we generalize these approaches, which are all based on linear embeddings. We learn a nonlinear representation of the input space jointly with the regression function. This allows to apply unsupervised dimensionality reduction as a byproduct of a supervised regression solution in a Bayesian framework. We also do not require any budget of samples prior starting the actual optimization.

Further work in high-dimensional BO has been devoted to decompose the problem into sub-problems featuring an additive structures. Kandasamy et al. (2015) decompose the input space into disjoint subsets of dimensionality at most d and optimizes the respective acquisitions independently. Extensions of this decomposition strategy that feature overlapping groups of dimensions and optimize the acquisition function via message passing protocols have been proposed in (Rolland et al., 2018; Hoang et al., 2017). In our work, we avoid restricting the input space to an axis-aligned representation and relax the additivity assumption of the objective function. Also the work of Li et al. (2016) removes axis-aligned constraint at the cost of less data efficient search in an over-sized box domain.

High-dimensional data often lives on a low-dimensional manifold, and in this paper we exploit exactly this idea to devise a BO algorithm that operates in high dimensions. More specifically, we propose to represent the probabilistic surrogate model in the following way: we learn a low-dimensional embedding of the original data space and a probabilistic mapping from this low-dimensional manifold to the observation space jointly. For the embedding, we use a multi-layer neural network, and for the probabilistic model we use a Gaussian process (Calandra et al., 2016; MacKay, 1998). This allows addressing the curse of dimensionality in black-box optimization problems by jointly learning a feature mapping $\mathbf{h}: \mathbb{R}^D \rightarrow \mathbb{R}^d$ of the input space jointly with the response surface f . We therefore propose a Bayesian optimization algorithm which maximizes the acquisition function in the embedded space. Moreover, we address the problem of data-efficiently learning an inverse mapping, $\mathbf{s}: \mathbb{R}^d \rightarrow \mathbb{R}^D$, to be able to reconstruct points in the original input domain after maximizing the acquisition.

Examples of nonlinear embeddings include Manifold Gaussian processes (Calandra et al., 2016), which resembles the problem of learning the surrogate model by reducing the dimensionality of the input space implicitly in the kernel. In our work, we follow a similar approach to the regression problem but we integrate the learning of the nonlinear embedding with that of an inverse mapping \mathbf{s} that allows for reconstructing inputs in the original domain from embedded locations. A similar encoder-decoder structure for a Bayesian optimization approach in high dimensions has been proposed also in (Gomez-Bombarelli et al., 2018) for optimizing over discrete molecules. Albeit careful modeling of the continuous optimization space, the deep models employed for the encoder and decoder require large amounts of data and hyper-parameters to tune such as convolution (e.g. *depth*, *width* and *growth factor* for the network) and middle-layer (e.g. *growth factor*) parameters. This formulation does not allow for calibrated uncertainty quantification in reconstructed space and suffers from data inefficiency due to a selection of parameters applied in a non Bayesian framework.

2. Problem Statement

We address the problem of minimizing a high-dimensional function $f: \mathcal{X} = [0, 1]^D \rightarrow \mathbb{R}$ and we assume that this problem has low *effective dimensionality* corresponding to $d \ll D$, i.e., we seek

$$\mathbf{x}_{opt} = \arg \min_{\mathbf{x} \in \mathcal{X}} f_{\mathcal{X}}(\mathbf{x}). \quad (1)$$

We assume we do not have access to an analytic form of $f_{\mathcal{X}}$ and can only observe values of the objective function corrupted by i.i.d. Gaussian noise, that is $y = f_{\mathcal{X}}(\mathbf{x}) + \varepsilon$, where $\varepsilon \sim \mathcal{N}(0, \sigma_n^2)$. Furthermore, no gradient information is available and we cannot make any assumption about the convexity of the function.

2.1. Encoder-decoder Bayesian Optimization

For the optimization of an intrinsically lower-dimensional unknown objective function we consider an *encoder-decoder* approach to learn a *response surface* in feature space from high-dimensional inputs $\mathbf{X} = \{\mathbf{x}_1, \dots, \mathbf{x}_N\} \subset \mathcal{X}$. The *encoder* transforms the input space \mathcal{X} with a parametric nonlinear mapping $\mathbf{h}: \mathbb{R}^D \rightarrow \mathbb{R}^d$ to the feature space denoted by $\mathcal{Z} \subset \mathbb{R}^d$. The nonlinear mapping allows defining a set of embedded points $\mathbf{Z} = \{\mathbf{z}_1, \dots, \mathbf{z}_N\} \subset \mathcal{Z}$ and the observations $\mathbf{y} = \{y_1, \dots, y_N\}$ identify the inputs and outputs of a low-dimensional response surface, $f_{\mathcal{Z}}: \mathcal{Z} \rightarrow \mathbb{R}$, which is usually modeled as a Gaussian process. An *acquisition function* $\alpha: \mathcal{Z} \rightarrow \mathbb{R}$ characterizes the most valuable locations to be selected for data-efficient optimization by trading-off exploration and exploitation of the response sur-

Algorithm 1 Encoder-Decoder BO

```

1: Input:  $\mathbf{X}_0 = \{\mathbf{x}_1, \dots, \mathbf{x}_N\}$ 
2: Observations:  $\mathbf{y}_0 = \{y_1, \dots, y_N\}$ 
3: for  $t = 0, 1, 2, \dots$  do
4:   Encode inputs  $\mathbf{Z}_t = \mathbf{h}(\mathbf{X}_t)$ 
5:   Learn response surface  $p(f_Z | \mathbf{Z}_t, \mathbf{y}_t)$ 
6:   Select  $\mathbf{z}_{t+1} = \operatorname{argmax}_{\mathbf{z} \in \mathcal{Z}} \alpha(\mathbf{z} | p(f_Z | \mathbf{Z}_t, \mathbf{y}_t))$ 
7:   Decode new design  $\mathbf{x}_{t+1} = \mathbf{s}(\mathbf{z}_{t+1})$ 
8:   Evaluate objective  $y_{t+1} = f_X(\mathbf{x}_{t+1}) + \varepsilon$ 
9:   Augment data  $\mathbf{X}_{t+1} = \mathbf{X}_t \cup \{\mathbf{x}_{t+1}\}, \mathbf{y}_{t+1} = \mathbf{y}_t \cup \{y_{t+1}\}$ 
10: end for
11: Return  $\mathbf{x}_{opt} = \arg \min \mathbf{y}_t$ 

```

. Algorithm 1: Main steps of the encoder-decoder Bayesian optimization algorithm. The dimensionality reduction step and the mapping to the original domain are explicitly represented in lines 4, 7, respectively. The main benefits of the dimensionality reduction step are that learning the response surface and optimization of the acquisition function happen in a lower-dimensional feature space.

face. The acquisition function assigns a score by looking at the predictions from the probabilistic surrogate model, $p(f_Z | \mathbf{Z}, \mathbf{y})$. It compensates highly uncertain predictions with low expected value for each location \mathbf{z} and it is maximized to define the point \mathbf{z}_{t+1} to be sampled at the next iteration:

$$\mathbf{z}_{t+1} = \operatorname{argmax}_{\mathbf{z} \in \mathcal{Z}} \alpha(\mathbf{z}) \quad (2)$$

In our work, we focus on a few classical examples of acquisition strategies that correspond to *Expected Improvement* (EI) (Močkus, 1975), *Probability of Improvement* (PI) (Kushner, 1964) and *Upper Confidence Bound* (UCB) (Srinivas et al., 2010). For a full review on available acquisitions for Bayesian optimization we refer to (Shahriari et al., 2016). The new location is in feature space and needs to be mapped back to the original domain \mathcal{X} in order to evaluate the high-dimensional objective at \mathbf{x}_{t+1} . We therefore include a mapping $\mathbf{s}: \mathbb{R}^d \rightarrow \mathbb{R}^D$ to reverse the effects of the encoder, that we refer to as *decoder*. The main steps of the encoder-decoder Bayesian optimization are described in Algorithm 1.

2.2. Gaussian Processes

We aim at learning a response surface with a probabilistic model that explicitly accounts for model parameter uncertainty and provides well-calibrated uncertainty bounds. The former characteristic enhances data efficiency as it is less prone to model errors than deterministic models; the latter characteristic is a desirable property that allows us

to exploit the posterior predictive distribution for exploring the optimization landscape. Gaussian processes (GPs) (Rasmussen & Williams, 2006) are the state-of-the-art for non-parametric method for nonlinear probabilistic regression. GPs are a distribution over functions and the GP prior is fully specified by a *mean function*, $m: \mathcal{X} \rightarrow \mathbb{R}$, and a *covariance function (kernel)* $k: \mathcal{X} \times \mathcal{X} \rightarrow \mathbb{R}$, which defines the covariance between function values as a function of the corresponding inputs. In our work, we model our unknown objective with a Gaussian process, that is $f_X \sim \mathcal{GP}(m, k)$. We consider Gaussian likelihoods, i.e., we assume each observation is corrupted by i.i.d. Gaussian noise, $\varepsilon \sim \mathcal{N}(0, \sigma_n^2)$. Then, the GP posterior predictive distribution at test point \mathbf{x}_* is Gaussian, i.e. $p(f_X(\mathbf{x}_*) | \mathbf{X}, \mathbf{y}) = \mathcal{N}(\mu_{GP}(\mathbf{x}_*), \sigma_{GP}^2(\mathbf{x}_*))$ where the mean and the variance are given by

$$\mu_{GP}(\mathbf{x}_*) = m_* + \mathbf{k}_*^T (\mathbf{K} + \sigma_n^2 \mathbf{I})^{-1} (\mathbf{y} - \mathbf{m}_x) \quad (3)$$

$$\sigma_{GP}^2(\mathbf{x}_*) = k_{**} - \mathbf{k}_*^T (\mathbf{K} + \sigma_n^2 \mathbf{I})^{-1} \mathbf{k}_*, \quad (4)$$

respectively. Here, \mathbf{I} is the identity matrix, m_* and \mathbf{m}_x are the mean function computed at test point and training inputs respectively. The term $\mathbf{k}_* = [k(\mathbf{x}_i, \mathbf{x}_*)]_{i=1}^N$ is the vector of covariance between function values evaluated at the training and test inputs, respectively, $\mathbf{K} = [k(\mathbf{x}_i, \mathbf{x}_j)]_{i,j}$ denotes the kernel matrix, and $k_{**} = k(\mathbf{x}_*, \mathbf{x}_*)$.

2.3. Multiple-output Gaussian Processes

In our encoder-decoder setting we are interested in modeling the relationship between the low-dimensional embedding and the original high-dimensional domain with a data-efficient model. Specifically, we aim at learning a functional relationship between a feature space $\mathcal{Z} \subset \mathbb{R}^d$ and an output space $\mathcal{X} \subset \mathbb{R}^D$ (which characterizes the input space of our original optimization problem (1)), where each dimension is possibly related to the other components. With multi-output Gaussian processes (MOGP) (Alvarez et al., 2011; Alvarez & Lawrence, 2011; Yu et al., 2009; Osborne et al., 2008) we formalize the correlation between outputs to improve prediction accuracy assuming that a vector-valued function $\mathbf{g} = \{g_m\}_{m=1}^D$ is a sample from a vector valued Gaussian process, that is $\mathbf{g} \sim \mathcal{GP}(\mathbf{m}, \mathbf{K})$. A multi-output Gaussian process is characterized by a vector of mean functions $\mathbf{m} = \{m_m\}_{m=1}^D$ and a positive matrix-valued function modeling the degree of correlation between the output dimensions and the data points, i.e. $[\mathbf{K}(\mathbf{z}, \mathbf{z}')]_{m,m'} = k_R((\mathbf{z}, m)(\mathbf{z}', m'))$ where k_R is a kernel defined on the joint space of inputs and output dimensions $\mathcal{Z} \times \{1, \dots, D\}$. Different formulations of the covariance function correspond to different generative model assumptions regarding the multiple outputs. Here we will consider the covariance structure of the *Intrinsic Coregionalization Model* (ICM) (Goovaerts, 1997), which allows great computational advantages in the calculation of the covariance

matrix by exploiting the properties of the Kronecker product. The ICM represents each output function as a linear combination of GP samples

$$g_m(\mathbf{z}) = \mathbf{a}_m^T \mathbf{u}(\mathbf{z}), \quad (5)$$

where the P -dimensional vector $\mathbf{u}(\mathbf{z}) = \{u^i(\mathbf{z})\}_{i=1}^P$ contains P functions randomly drawn from the GP prior $\mathcal{GP}(m(\cdot), k(\cdot, \cdot))$ such that $u^i(\mathbf{z}) \sim \mathcal{N}(m(\mathbf{z}), k(\mathbf{z}, \mathbf{z}))$ for $i = 1, \dots, P$, and $\mathbf{a}_m \in \mathbb{R}^P$ are hyper-parameters of the model to be learned from data. Collecting all outputs of the vector-valued function $\mathbf{g}(\mathbf{z})$ and all the linear coefficients in a matrix $\mathbf{A} = [\mathbf{a}_1, \dots, \mathbf{a}_D]^T \in \mathbb{R}^{D \times P}$, such that $\mathbf{g}(\mathbf{z}) = \mathbf{A}\mathbf{u}(\mathbf{z})$, the resulting covariance becomes

$$\text{Cov}(\mathbf{g}(\mathbf{z}), \mathbf{g}(\mathbf{z}')) = \mathbf{B} k(\mathbf{z}, \mathbf{z}') \quad (6)$$

where the $\mathbf{B} \in \mathbb{R}^{D \times D}$ is a positive semi-definite matrix defined as $\mathbf{B} = \mathbf{A}\mathbf{A}^T$ whose rank is determined by the number of latent functions P and which is referred to as *coregionalization matrix* (Alvarez et al., 2011). In the following, we will restrict ourselves to the *isotopic* case for which the same input set $\mathbf{Z} = \{\mathbf{z}_1, \dots, \mathbf{z}_N\}$ is shared across all output functions \mathbf{g} and will use data-sets like $S_m = \{(\mathbf{z}_1, x_{m,1}), \dots, (\mathbf{z}_N, x_{m,N})\}$ in order to learn function g_m for $m = 1, \dots, D$.

3. GP Autoencoder

In this section, we develop a data-efficient encoder-decoder model for learning embedded representations of high-dimensional BO inputs using Gaussian processes. The model will include an encoder part and decoder part that will be trained within a Bayesian framework. An illustration of the joint model is also depicted in Figure 1.

3.1. Manifold GP Encoder

In the first part of our optimization in Algorithm 1, we aim at transforming the input space \mathcal{X} with a parametric nonlinear mapping \mathbf{h} and subsequently model a response surface f_Z in a lower-dimensional space. The manifold Gaussian process (mGP) (Calandra et al., 2016; MacKay, 1998) addresses this challenge with a single GP model by jointly learning the composition of the feature mapping with the low-dimensional representation of the objective, i.e. the function $(f_Z \circ \mathbf{h})$. As the parametric feature mapping \mathbf{h} we use a multi-layer neural network

$$\mathbf{h}(\mathbf{X}) = (\mathbb{L}_l \circ \dots \circ \mathbb{L}_1)(\mathbf{X}) \quad (7)$$

with l being the total number of layers and where each layer $\mathbb{L}_i(\mathbf{X}) = \varphi(\mathbf{W}_i \mathbf{X} + \mathbf{V}_i)$ applies an activation function φ after an affine transformation of the input units with weights, \mathbf{W}_i , and biases, \mathbf{V}_i , for $i = 1, \dots, l$. The manifold Gaussian

process $\mathcal{GP}(\hat{m}(\cdot), \hat{k}(\cdot, \cdot))$ is defined by embedding the neural network in the covariance function such that the mGP kernel operates on high-dimensional inputs in \mathcal{X} , i.e.

$$\hat{k}(\mathbf{x}, \mathbf{x}') = k(\mathbf{h}(\mathbf{x}), \mathbf{h}(\mathbf{x}')). \quad (8)$$

This means the kernel k introduces regularity assumptions about the underlying function, such as smoothness or periodicity, while the \hat{k} covariance also implies that the high-dimensional function is actually controlled by inputs on a lower-dimensional manifold. This parametric mapping allows applying dimensionality reduction in a Bayesian framework since the parameters of the neural network $\theta_h = [\mathbf{W}_1, \dots, \mathbf{W}_l, \mathbf{V}_1, \dots, \mathbf{V}_l]$ are treated as hyper-parameters $\hat{\theta} = (\theta_h, \theta_k)$ of the kernel \hat{k} and can jointly be optimized via marginal likelihood maximization, where the θ_k denotes the hyper-parameters of the kernel k . One advantage with the neural network model is to capture correlations between dimensions in feature space \mathcal{Z} since a hidden layer of units is shared between inputs and outputs (Wilson et al., 2011). Other manifold learning techniques (Belkin & Niyogi, 2002; Saul & Roweis, 2003) to represent \mathbf{h} , such as PCA (Pearson, 1901; Jolliffe, 2011) would only provide an unsupervised parsimonious representation of \mathcal{X} based on maximum variance in the feature space, thereby neglecting the functional relationship between \mathbf{X} and \mathbf{y} .

The objective when training the manifold GP is the log-marginal likelihood $\log p(\mathbf{y}|\mathbf{X}, \hat{\theta})$

$$\log p(\mathbf{y}|\mathbf{X}, \hat{\theta}) = -\frac{1}{2}\mathbf{y}^T \hat{\mathbf{K}}_y^{-1} \mathbf{y} - \frac{1}{2} \log |\hat{\mathbf{K}}_y| - \frac{N}{2} \log 2\pi, \\ \hat{\mathbf{K}}_y = \hat{\mathbf{K}} + \sigma_n^2 \mathbf{I} \quad (9)$$

where $\hat{\mathbf{K}} = [\hat{k}(\mathbf{x}_i, \mathbf{x}_j)]_{i,j}$, for $i, j = 1, \dots, N$. To train the manifold GP, we maximize the log-marginal likelihood. The manifold GP posterior predictions are equivalent to the ones presented in equations (3) and (4), respectively, if we use \hat{k} as the kernel.

3.2. Multi-output GP Decoder

In our BO approach we need to evaluate designs selected in feature space on a high-dimensional objective function. A necessary transformation is therefore a mapping from the embedded representation \mathcal{Z} to the original domain \mathcal{X} , where the objective function f_X for our originally expensive high-dimensional experiments is defined. We use a multi-output Gaussian process for the decoder, which allows for sharing information between output dimensions, capturing correlations between coordinates $\{x_i\}_{i=1}^D$. Employing MOGPs for mapping to a high-dimensional space, however, raises a series of challenges. Given a dataset of (input-outputs) $(\mathbf{Z} \in \mathbb{R}^{N \times d}, \mathbf{X} \in \mathbb{R}^{N \times D})$ the full covariance matrix \mathbf{K} describing the correlation between observations in each single

output and cross-correlations between different outputs is the result of a Kronecker product

$$\bar{\mathbf{K}} = \mathbf{B} \otimes \mathbf{K}(\mathbf{Z}, \mathbf{Z}) \quad (10)$$

according to the intrinsic coregionalization model (Goovaerts, 1997), the matrix $[\mathbf{K}(\mathbf{Z}, \mathbf{Z})]_{i,j} = k(\mathbf{z}_i, \mathbf{z}_j)$, for $i, j = 1, \dots, N$ with kernel k is the covariance matrix of the latent Gaussian process sampled to generate the multiple outputs, and \mathbf{B} is the coregionalization matrix. MOGP training and prediction require Cholesky decomposition of the matrix $\bar{\mathbf{K}} \in \mathbb{R}^{ND \times ND}$, with complexity $\mathcal{O}(D^3 N^3)$, which becomes intractable for large D or N .

Hierarchical ICM To scale our decoder to high-dimensional outputs, we introduce an approximation based on a partitioning of the output space. We divide the domain of the high-dimensional objective in Q axis-aligned projections containing at most d_{MO} dimensions each, i.e. $\mathcal{X} = \mathcal{X}_1 \times \dots \times \mathcal{X}_Q$, where each $\mathcal{X}_i \subset \mathbb{R}^{d_{MO}}$, so that $\mathcal{X}_i \cap \mathcal{X}_j = \emptyset$ for $i \neq j$, with $\cup_{i=1}^Q \mathcal{X}_i = \mathcal{X}$. In this setting, we assume independence between vector outputs of different low-dimensional spaces

$$\text{Cov}(\mathbf{x}_i, \mathbf{x}_j) = \mathbf{0}, \quad \mathbf{x}_i \in \mathcal{X}_i, \mathbf{x}_j \in \mathcal{X}_j, i \neq j. \quad (11)$$

This allows us to model the D outputs with a hierarchy of ICMs (HICM). In particular, we define Q independent multi-output GPs to learn a set of vector valued functions $\mathbf{g}_i: \mathcal{Z} \rightarrow \mathcal{X}_i$, for $i = 1, \dots, Q$. Given a set of inputs \mathbf{Z} and a set of high-dimensional observations \mathbf{X} , under Gaussian likelihood we can rewrite the joint covariance matrix of our observations as a block-diagonal matrix $\bar{\mathbf{K}}_H$

$$\bar{\mathbf{K}}_H = \begin{pmatrix} \bar{\mathbf{K}}_1 & & & \\ & \bar{\mathbf{K}}_2 & & \\ & & \ddots & \\ & & & \bar{\mathbf{K}}_Q \end{pmatrix} \quad (12)$$

where each matrix $\bar{\mathbf{K}}_i = \mathbf{B}_i \otimes \mathbf{K}_i(\mathbf{Z}, \mathbf{Z}) + \sigma_n^2 \mathbf{I}$ is the result of an intrinsic coregionalization model with kernel k_i and hyper-parameters $[\mathbf{B}_i, \theta_i]$, with θ_i being the kernel hyper-parameters, for $i = 1, \dots, Q$. The advantage with this new approach is that each coregionalization matrix has now dimensions $d_{MO} \times d_{MO}$. This translates in a more efficient decomposition of each covariance block. The complexity of decomposing the block-diagonal covariance $\bar{\mathbf{K}}_H$ becomes $\mathcal{O}(Q d_{MO}^3 N^3)$, which scales linearly with the number of partitions and has bounded $d_{MO} \leq 3$. Given this structure for the multi-output decoder we define the feature mapping \mathbf{s} as the union of posterior means obtained by the hierarchical coregionalization model, that is $\mathbf{s}(\mathbf{z}) = \cup_{i=1}^Q \{\mu_i(\mathbf{z})\}$.

3.3. GP Encoder-Decoder Model

Finally, we train jointly the GP encoder and the multi-output GP decoder in order to maximize a shared objective with

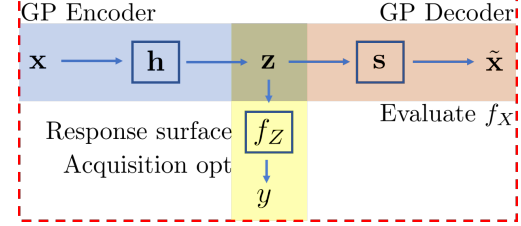


Figure 1. Full description of the GP autoencoder model. The blue box identifies the feature mapping with a multi-layer neural network embedded in the kernel of the mGP. The yellow body describes the learned function for BO in feature space. The brown box describes the mapping essential to evaluate the true objective f_X at the inputs \mathbf{x}_{t+1} that correspond to the optimal designs \mathbf{z}_{t+1} in feature space.

respect to all the parameters of the model θ_A . With this approach the weights and biases of the manifold GP would be calibrated taking into account a multi-dimensional mapping with output correlations. The objective that we optimize is the joint log-marginal likelihood $\log(p(\mathbf{y}, \tilde{\mathbf{X}} | \mathbf{X}, \theta_A))$ of the joint multi-output model

$$\mathbf{X} \xrightarrow{\mathbf{h}} \mathbf{Z} \xrightarrow{\text{HICM}} \begin{bmatrix} \tilde{\mathbf{X}} \\ \mathbf{y} \end{bmatrix}, \quad (13)$$

where the $\tilde{\mathbf{X}}$ denotes the reconstructed inputs of the autoencoder. In this model, the observations of the manifold GP are included as an additional output, without cross covariance, of a vector-valued GP. It is intuitive to avoid modeling correlations between outputs \mathbf{y} and input dimensions $\{\tilde{x}_i\}_{i=1}^D$ since they represent two completely different tasks and therefore could be assigned independent GP models.

Training Under these modeling assumptions, the joint log-marginal likelihood is given as

$$\log(p(\mathbf{y}, \tilde{\mathbf{X}} | \mathbf{X}, \theta_A)) = -\frac{1}{2} \mathbf{y}^T \hat{\mathbf{K}}_y^{-1} \mathbf{y} - \frac{1}{2} \log |\hat{\mathbf{K}}_y| - \frac{1}{2} \mathbf{x}_V^T \bar{\mathbf{K}}_H^{-1} \mathbf{x}_V - \frac{1}{2} \log |\bar{\mathbf{K}}_H|, \quad (14)$$

where the matrices $\hat{\mathbf{K}}_y$ and $\bar{\mathbf{K}}_H$ have been defined in Equations (9) and (12), respectively. The vector $\mathbf{x}_V \in \mathbb{R}^{ND}$ is obtained by stacking all columns of the dataset \mathbf{X} .

4. Experiments

In this section, we assess whether the proposed model can learn sensible representations of objective functions that improve sample efficiency and accuracy of high-dimensional BO. We expect our GP autoencoder-based optimization to be suitable with high-dimensional functions that only depend on a low-dimensional manifold of their domain. We formulate our assumption of effective low dimensionality

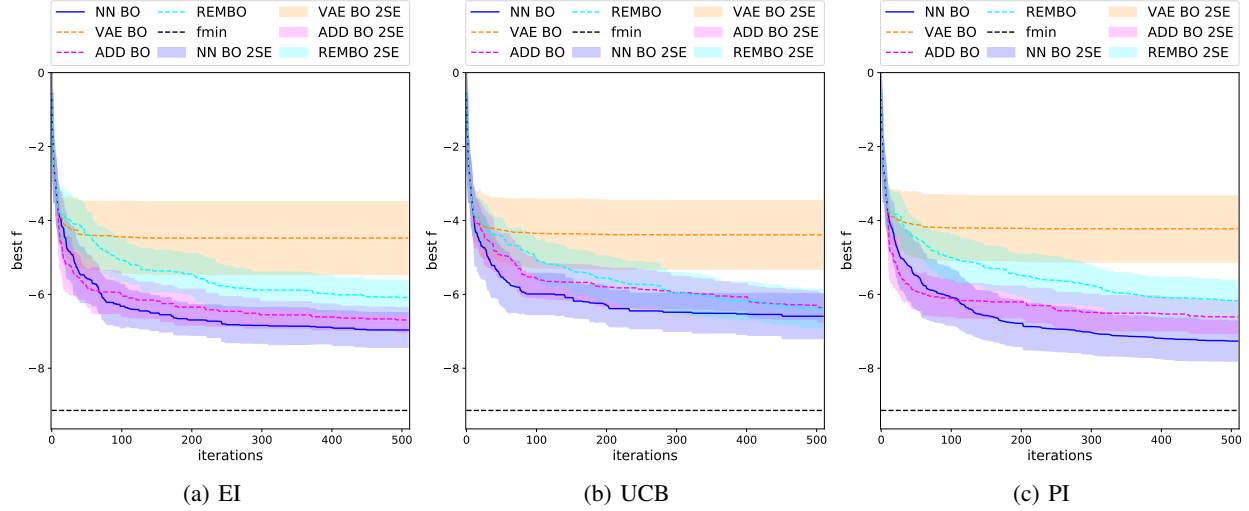


Figure 2. Results of BO optimization with the additive Michalewicz benchmark function. Each figure shows convergence results for a different choice of acquisition function: EI 2(a), UCB 2(b) and PI 2(c). Confidence bounds are obtained from standard error over 20 different initializations for each baseline. The manifold BO baseline (NN-BO) obtains identical or better performances w.r.t. ADD-BO which conforms to additivity structure of the objective.

by introducing a linear mapping on all objective functions used in this section

$$f_X(\mathbf{x}) = f(\mathbf{O}\mathbf{x}) \quad (15)$$

where the matrix $\mathbf{O} \in \mathbb{R}^{d \times D}$ projects the high-dimensional \mathbf{x} to a linear subspace where the benchmark function f is evaluated. The entries of the projection matrix are samples from a standard Gaussian with zero mean and unit variance, and care is taken to ensure that the optimum is contained in the interval $[0, 1]^D$, that is $\exists \mathbf{x} \in [0, 1]^D$ such that $\mathbf{O}\mathbf{x} = \mathbf{z}^*$, with \mathbf{z}^* being the minimizer of the benchmark function f .

As comparing baselines we select the *variational deep autoencoder* based BO (VAE-BO) (Gomez-Bombarelli et al., 2018), which trains a deep network for both the encoder \mathbf{h} and the decoder \mathbf{s} , and then applies a GP regression in feature space to model the relationship between low-dimensional inputs and observations. In our experiments, the training of the deep network is executed prior starting the BO optimization by minimizing the mean squared reconstruction error with 500 data points. This setting exploits an additional budget of input-outputs in order to provide enough information for the data-costly model. We further compare our method to *additive models* based BO (ADD-BO) (Kandasamy et al., 2015) and *random embeddings* (REMBO) (Wang et al., 2013). For our baseline (NN-BO) we employ a 3-layer neural network embedded in the kernel with $D - 20 - d$ units.

We consider a set of benchmarks with known analytic forms in order to extend the analysis of our BO approach to a set of different properties, such as additivity with disjoint and

overlapping groups of dimensions. In all our experiments, we select the Matern_{5/2} covariance function for all GP regressions and normalized inputs and outputs for the training in our experiments. For more conclusive results, we also evaluate the models on three different acquisition function, *expected improvement* (EI) (Močkus, 1975), *probability of improvement* (PI) (Kushner, 1964) and *upper confidence bound* (UCB) (Srinivas et al., 2010). The maximization of the acquisition function is performed selecting the highest 100 locations out of 5000 uniformly random samples and then applying bounded gradient based L-BFGS-B optimizer (Lu et al., 1994; Zhu et al., 1997) to the best points. All baselines feature the same strategy for optimization of the acquisition function.

Each optimization experiment is repeated over 20 different random initializations to compute the mean estimate and the error bars of each baseline. All experiments have a budget of queries that is set to 500 with 10 starting input-output pairs at the first BO iteration.

4.1. Additive with independent components

In this experiment, we assess the performances of the autoencoder GP model with a high-dimensional version of the Michalewicz function. We consider a 60-dimensional input space and we reduce it to its original dimensionality $d = 10$. This benchmark function (in feature space) is characterized by one-dimensional additive components defined on disjoint

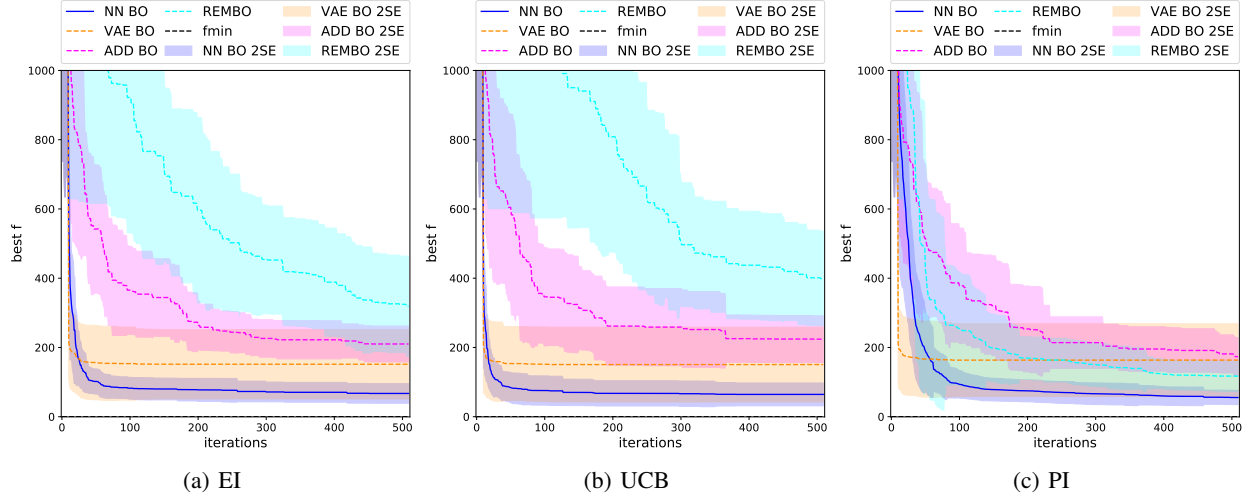


Figure 3. Results of BO optimization with the additive Rosenbrock benchmark function characterized by overlapping groups of dimensions. Different acquisition choices are shown to avoid over-fitting to a single exploration strategy: EI 3(a), UCB 3(b), PI 3(c). Curves show the mean and standard error of optimization progression over 20 initializations. Baselines that learn a low-dimensional manifold, namely NN-BO and VAE-BO show steepest convergence for all acquisitions, while REMBO requires greedy optimization steps with PI acquisition to converge to better optimum.

subsets of features

$$f(\mathbf{z}) = \sum_{i=1}^d -\sin(z_i) \sin^{2m} \left(\frac{iz_i^2}{\pi} \right), \quad (16)$$

where m is a parameter that characterizes the steepness of the local minima and maxima of f and is set to $m = 0.5$ for our problem. We embed the benchmark function in a 60-dimensional space ($D = 60$). Figure 2 shows the best observations collected during the optimization history. The GP autoencoder baseline shows a slow descent during the early stages of the optimization compared to ADD-BO which needs to learn a simpler feature representation of f . After 100 BO iterations NN-BO recovers the best descent and lowest observed value at termination across all acquisition functions. This can be explained by an improvement of accuracy of the feature space learning after seeing enough input-output pairs. The convergence curve of ADD-BO and REMBO also show competitive performances, while REMBO features a slower exploration due to the linear dimensionality reduction, which allows for exploration of the input space in d fixed directions of the high-dimensional input space per BO iteration. The worst performances correspond to the VAE-BO. The 500 inputs-outputs for training the deep model were insufficient to learn an accurate mapping from feature space to the high-dimensional domain. For most embedded points only slight modifications are observed after the mapping $s(\mathbf{z})$. The poor reconstruction task highly penalizes exploration in the reconstructed space.

4.2. Additive with overlapping components

Another category of objectives is characterized by additive maps whose additive function components share dimensions between their low-dimensional input spaces. In this experiment, we consider the Rosenbrock function as an example for introducing correlations between the additive components and for assessing the capability of our GP autoencoder model to capture steep descents in feature space. The Rosenbrock function is defined as

$$f(\mathbf{z}) = \sum_{i=1}^{d-1} [100(z_{i+1} - z_i^2)^2 + (z_i - 1)^2] \quad (17)$$

and is a common choice for testing gradient-based optimization methods due to its unimodal shape. Our purpose with the BO approach is to show the extremely efficient learning capability of feature-space methods, even when embedding the function in 60 dimensions. We assume in this experiment a feature space of $d = 10$ dimensions and optimize within a budget of 500 BO iterations. Figure 3 shows the descent toward the optimum obtained with each baseline. Both manifold learning based approaches, namely NN-BO and VAE-BO, show the best performances denoting high data efficiency in representing a parabolic valley-shaped function despite its linear embedding in a high-dimensional space. The NN-BO model features fast descents in the early stages of optimization and best value observed at termination consistently outperforming the other baselines across all acquisition functions. The additive model optimization ADD-BO and REMBO suffer from slower exploration. The linear embedding penalizes the axis-aligned decomposition

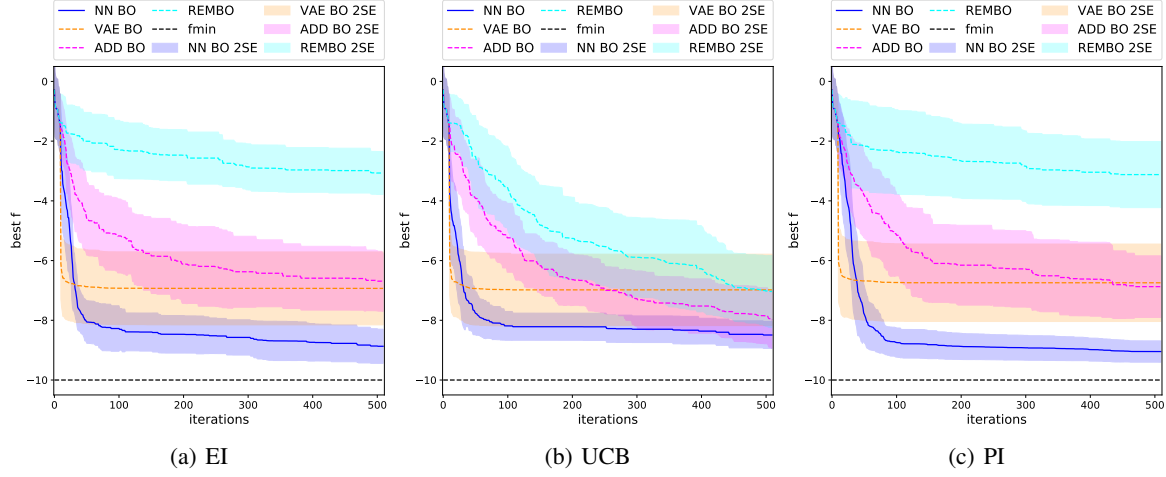


Figure 4. Progression of Bayesian optimization with the non additive Product of Sines function which can be decomposed as a product of low-dimensional functions. Small variations in the outputs of the decoder for NN-BO and VAE-BO restrict exploration after the early stages of optimization. The NN-BO baseline, however, shows steepest descent and best value at termination as a result of the data efficient learning of the embedded representation.

of the additive model, which also assumes independence between the additive components. It features high sensitivity w.r.t. the choice of the acquisition function, leveraging a more greedy exploration in relatively small steps.

4.3. Non additive high-dimensional objectives

In our last experiment, we consider a low-dimensional objective defined as the product of sine functions. In this setting, we aim at assessing the quality of the manifold learning and multi-output GP decoding when the function f is not additive and therefore does not conform to the ADD-BO baseline assumptions. We define the low-dimensional objective as a product of scalar functions:

$$f(\mathbf{z}) = 10 \sin(z_1) \prod_{i=1}^d \sin(z_i). \quad (18)$$

We embed it in high dimensional space via linear mapping where $D = 60$ and execute the optimization in a 10-dimensional feature space. Figure 4 compares the succession of optimal observations (with standard errors). The ADD-BO baseline shows a much slower descent in the early stages of optimization. It recovers an optimal value at termination that is close to the GP autoencoder baseline only for a single choice of acquisition function. UCB is shows the most aggressive exploration. Both manifold learning baselines show steep descent during the early stages of the optimization, with slower exploration after the first 50 iterations. This effect is due to small variations in the outputs of the decoder mapping for both manifold BO approaches. In particular, in the GP autoencoder baseline, a too aggressive exploration in feature space can lead to designs that are far

away from the data obtained up to this point. This causes the GP decoder to fall back to the prior and produce posterior mean predictions that are close to zero for many optimally selected embedded points. REMBO shows slowest convergence and recovers competitive performances w.r.t. other baselines only for one choice of acquisition function. In this example, the selection of the linear projection matrix for the random embedding baseline is key for performances of optimization.

5. Conclusion

We presented an approach for scaling Bayesian optimization to high-dimensional input spaces for problems characterized by a low effective dimensionality of the objective function. We proposed a generalization of existing BO techniques based on nonlinear subspace optimization and learning. In particular, we directly formulated the learning of the dimensionality reduction mapping and regression problem in a single joint model. We finally addressed the curse of dimensionality in multi-output Gaussian process predictions by introducing independence assumptions between groups of dimensions in output space. We argue that the great advantage introduced with the GP autoencoder is the data efficiency for learning the low-dimensional representation of the objective and the decoder mapping from feature space to high-dimensions. The GP autoencoder can efficiently learn a sensible representation that is effective for optimization. Based on experimental results, we observe that this approach is suitable for high-dimensional optimization independently of the decomposition properties of the low-dimensional objective function.

References

Alvarez, M. A. and Lawrence, N. D. Computationally efficient convolved multiple output Gaussian processes. *The Journal of Machine Learning Research*, 2011.

Alvarez, M. A., Rosasco, L., and Lawrence, N. D. Kernels for vector-valued functions: a review. *Foundations and Trends in Machine Learning*, 2011.

Belkin, M. and Niyogi, P. Laplacian eigenmaps and spectral techniques for embedding and clustering. *Advances in Neural Information Processing Systems*, 2002.

Calandra, R., Peters, J., Rasmussen, C. E., and Deisenroth, M. P. Manifold Gaussian processes for regression. *International Joint Conference on Neural Networks IEEE*, 2016.

Chen, B., Castro, R. M., and Krause, A. Joint optimization and variable selection of high-dimensional Gaussian processes. *International Conference on Machine Learning*, 2012.

Djolonga, J., Krause, A., and Cevher, V. High-dimensional Gaussian process bandits. *Advances in Neural Information Processing Systems*, 2013.

Garnett, R., Osborne, M. A., and Hennig, P. Active learning of linear embeddings for Gaussian processes. 2013.

Gomez-Bombarelli, R., Jennifer, N. W., Duvenaud, D., Hernndez-Lobato, J. M., Snchez-Lengeling, B., Sheberla, D., Aguilera-Iparraguirre, J., Hirzel, T. D., Adams, R. P., and Aspuru-Guzik, A. Automatic chemical design using a data-driven continuous representation of molecules. *ACS Central Science*, 2018.

Goovaerts, P. *Geostatistics for natural resources evaluation*. 1997.

Hoang, T. N., Hoang, Q. M., Ouyang, R., and Low, K. H. Decentralized high-dimensional Bayesian optimization with factor graphs. *Association for the Advancement of Artificial Intelligence*, 2017.

Hutter, F., Hoos, H. H., and Leyton-Brown, K. Sequential model-based optimization for general algorithm configuration. *Lecture Notes in Computer Science*, 2011.

Jolliffe, I. *Principal component analysis*. 2011.

Jones, D. R., Schonlau, M., and Welch, W. J. Efficient global optimization of expensive black-box functions. *Journal of Global Optimization*, 1998.

Kandasamy, K., Schneider, J., and Poczos, B. High dimensional Bayesian optimisation and bandits via additive models. *International Conference on Machine Learning*, 2015.

Kushner, H. J. A new method of locating the maximum point of an arbitrary multipeak curve in the presence of noise. *Journal of Basic Engineering*, 1964.

Li, C. L., Kandasamy, K., Poczos, B., and Schneider, J. High dimensional Bayesian optimization via restricted projection pursuit models. *International Conference on Artificial Intelligence and Statistics*, 2016.

Lu, P., Nocedal, J., Zhu, C., Byrd, R. H., and Byrd, R. H. A limited-memory algorithm for bound constrained optimization. *SIAM Journal on Scientific Computing*, 16: 1190–1208, 1994.

MacKay, D. J. Introduction to Gaussian processes. *NATO ASI Series F Computer and Systems Sciences*, 1998.

Močkus, J. On Bayesian methods for seeking the extremum. *Optimization Techniques IFIP Technical Conference*, 1975.

Osborne, M. A., Roberts, S. J., Rogers, A., Ramchurn, S. D., and Jennings, N. R. Towards real-time information processing of sensor network data using computationally efficient multi-output Gaussian processes. *International Conference on Information Processing in Sensor Networks*, 2008.

Pearson, K. On lines and planes of closest fit to systems of points in space. *The London, Edinburgh, and Dublin Philosophical Magazine and Journal of Science*, 1901.

Rana, S., Li, C., Gupta, S., Nguyen, V., and Venkatesh, S. High dimensional Bayesian optimization with elastic Gaussian process. *International Conference on Machine Learning*, 2017.

Rasmussen, C. E. and Williams, C. K. I. *Gaussian processes for machine learning*. 2006.

Rolland, P., Scarlett, J., Bogunovic, I., and Cevher, V. High-dimensional Bayesian optimization via additive models with overlapping groups. *International Conference on Artificial Intelligence and Statistics*, 2018.

Saul, L. K. and Roweis, S. T. Think globally, fit locally: unsupervised learning of low dimensional manifolds. *Advances in Neural Information Processing Systems*, 2003.

Shahriari, B., Swersky, K., Wang, Z., Adams, R. P., and De Freitas, N. Taking the human out of the loop: a review of Bayesian optimization. *IEEE*, 2016.

Snoek, J., Larochelle, H., and Adams, R. P. Practical Bayesian optimization of machine learning algorithms. *Advances in Neural Information Processing Systems*, 2012.

Srinivas, N., Krause, A., Kakade, S., and Seeger, M. W. Gaussian process bandits without regret: an experimental design approach. *International Conference on Machine Learning*, 2010.

Sui, Y., Gotovos, A., Burdick, J., and Krause, A. Safe exploration for optimization with Gaussian processes. *International Conference on Machine Learning*, 2015.

Wang, Z., Zoghi, M., Hutter, F., Matheson, D., and De Freitas, N. Bayesian optimization in high dimensions via random embeddings. *International Joint Conference on Artificial Intelligence*, 2013.

Wilson, A. G., Knowles, D. A., and Ghahramani, Z. Gaussian process regression networks. 2011.

Yu, B. M., Cunningham, J. P., Santhanam, G., Ryu, S. I., Shenoy, K. V., and Sahani, M. Gaussian process factor analysis for low-dimensional single-trial analysis of neural population activity. *Journal of Neurophysiology*, 2009.

Zhu, C., Byrd, R. H., Lu, P., and Nocedal, J. Algorithm 778: L-bfgs-b: Fortran subroutines for large-scale bound-constrained optimization. *ACM Transactions on Mathematical Software*, 1997.